

Self-consistent evolution of plasma discharge and electromagnetic fields in a microwave pulse compressor

A. S. Shlapakovski,¹ L. Beilin,¹ Y. Hadas,² E. Schamiloğlu,³ and Ya. E. Krasik¹

¹*Physics Department, Technion 32000 Haifa, Israel*

²*Department of Applied Physics, Rafael, POBox 2250, Haifa 31021, Israel*

³*Department of Electrical and Computer Engineering, University of New Mexico, Albuquerque, New Mexico 87131, USA*

(Received 13 May 2015; accepted 30 June 2015; published online 15 July 2015)

Nanosecond-scale evolution of plasma and RF electromagnetic fields during the release of energy from a microwave pulse compressor with a plasma interference switch was investigated numerically using the code MAGIC. The plasma was simulated in the scope of the gas conductivity model in MAGIC. The compressor embodied an S-band cavity and H-plane waveguide tee with a shorted side arm filled with pressurized gas. In a simplified approach, the gas discharge was initiated by setting an external ionization rate in a layer crossing the side arm waveguide in the location of the electric field antinode. It was found that with increasing ionization rate, the microwave energy absorbed by the plasma in the first few nanoseconds increases, but the absorption for the whole duration of energy release, on the contrary, decreases. In a hybrid approach modeling laser ignition of the discharge, seed electrons were set around the electric field antinode. In this case, the plasma extends along the field forming a filament and the plasma density increases up to the level at which the electric field within the plasma decreases due to the skin effect. Then, the avalanche rate decreases but the density still rises until the microwave energy release begins and the electric field becomes insufficient to support the avalanche process. The extraction of the microwave pulse limits its own power by terminating the rise of the plasma density and filament length. For efficient extraction, a sufficiently long filament of dense plasma must have sufficient time to be formed. © 2015 AIP Publishing LLC.

[<http://dx.doi.org/10.1063/1.4926819>]

I. INTRODUCTION

Microwave plasma discharges in pressurized gases have been extensively investigated for many years for a large range of pulse durations and frequencies. The basic phenomena involved in a microwave gas breakdown are described and relatively well understood.^{1,2} More recently, many experimental, theoretical, and numerical studies of the spatial structure and temporal evolution of plasma formed in the high-pressure microwave discharge have been performed.^{3–7} Yet, the dynamics of the plasma formation at the initial—nanosecond time-scale—stage of the discharge remains insufficiently understood. This is especially important for the case of discharge in a resonant cavity as there is a mutual influence of the discharge development and the process of microwave energy release from the cavity that goes out of resonance during plasma generation.

Such a situation directly concerns the operation of high-gain resonant microwave pulse compressors^{8,9} with plasma switches. In these compressors, the resonant cavity is charged by an external source; then the plasma discharge is initiated, the cavity is opened, and the stored energy is rapidly extracted into a load. High-gain compressors are a promising alternative to high-power microwave sources driven by relativistic electron beams since compressors can generate hundreds megawatt output power using well-developed megawatt-level magnetrons or klystrons capable of reliable operation at high repetition rates. For high power gain, the switch should open the cavity almost fully so that

the characteristic time of energy release approaches the round-trip time for a traveling electromagnetic wave along the cavity; usually, this is several nanoseconds.

The switch, therefore, is a key element for efficient compressor operation since the dynamics of plasma formation in it actually shapes the waveform of the microwave output pulse and ultimately determines the output power. Despite advances in the practical development of such compressors,¹⁰ the problem of the influence of plasma density evolution on the compressor output pulse was neither considered theoretically nor simulated numerically. Meanwhile, the importance of gaining a deeper understanding of the self-consistent dynamics of the plasma discharge and cavity fields for minimizing switching losses (2–3 dB at best in practice) and improving the quality of the output pulse (so far, output pulses of resonant compressors have rather triangular waveform) seems obvious.

The first attempt to simulate the process of the output pulse extraction from the resonant microwave compressor with the plasma switch was undertaken in our recent work.¹¹ Simulations were performed with the use of the fully electromagnetic particle-in-cell (PIC) code MAGIC (Ref. 12) for a simple rectangular waveguide-based geometry of the compressor using an H-plane waveguide tee as an interference switch. Different options for introducing the plasma provided by MAGIC were tried, and it was found that the gas conductivity model¹³ and hybrid model combining the plasma representation as a conductive gas with particles treated by the PIC algorithm are most appropriate for these

studies. It was shown that the rise of the compressor output power in time correlates with the rise of the plasma density. In addition, the output power rises with the expansion of the volume occupied by the plasma.

In this work, we continue studies started in Ref. 11 using the gas conductivity model for the plasma. We focus now on the issues important for understanding the factors determining the switching losses and the waveform of the output pulse, i.e., on the dynamics of the RF energy absorption in the plasma and on the self-consistent evolution of the plasma density and RF electric field in the compressor cavity and switch. In addition to the model configuration of the compressor, same as in Ref. 11, we have also performed simulations for the geometry of the compressor studied in our experimental works^{14–16} to compare the simulation results with those obtained in the experiments.

II. SIMULATED CONFIGURATIONS AND PLASMA MODEL

The simulations were performed for the geometry consisting of standard S-band rectangular waveguide sections (72 mm × 34 mm). Although compressors with a cylindrical cavity and switch design are capable of higher gain,¹⁰ the rectangular waveguide-based geometry is also employed elsewhere in experiments.^{17,18} The 3-D view of the system (with coordinate axes) is shown in Fig. 1 along with the x - y cross-sections and RF electric field patterns obtained in simulations of the compressor charging without plasma for two different cases: the model configuration, as in Ref. 11, and the experimental configuration, as in Refs. 14–16. The simulation region includes the input and output sections, a cavity section, and a shorted side arm; the total length is 144 cm in both cases. The waveguide walls are silver for the model configuration and brass for the experimental one. The input iris of 4 mm thickness has a circular coupling hole, 27 mm in diameter; for the case of the model configuration, it is filled with a dielectric of $\epsilon = 2.25$. At the input port, the electromagnetic wave in the TE₁₀ mode is injected into the system with a set amplitude of the RF voltage across the waveguide. The frequencies corresponding to resonant charging are 2980.2 and 2766.8 MHz for the model and experimental configurations, respectively.

The simulations of the stage of microwave energy release caused by the appearance of the plasma were initiated by the preset RF fields obtained in preliminary simulations of charging the compressors without plasma for the geometries presented in Fig. 1. The gas conductivity model embedded in MAGIC implies that the plasma is treated as a conductive gas whose conductivity is calculated from the electron and ion densities n and mobilities μ depending on the electric field and pressure

$$\sigma_{gas} = e(\mu_e n_e + \mu_p n_p + \mu_n n_n), \quad (1)$$

where indices e , p , n correspond to electrons, positive, and negative ions, respectively. The densities evolve according to the equations accounting for electron avalanche, electron-neutral attachment, electron-ion recombination, and positive-negative ion neutralization:

$$\begin{aligned} \frac{dn_e}{dt} &= Q_e + (\alpha - \beta)n_e - \alpha_e n_e n_p \\ \frac{dn_n}{dt} &= \beta n_e - \alpha_i n_n n_p \\ n_p &= n_e + n_n. \end{aligned} \quad (2)$$

Here, the coefficients α (avalanche), β (attachment), α_e (recombination), and α_i (neutralization) are set as functions of field and pressure. The source term Q_e (the rate of external ionization) can be set as a function of the spatial coordinates and time (no particles in a simulation) or, alternatively, is calculated using ionization cross-sections for primary particles (electrons) treated by the PIC algorithm

$$Q_e = \frac{qN}{e\Delta V} \sum_i v_i \sigma_{ion}(v_i), \quad (3)$$

where q and v_i are the charge and velocity of a macroparticle, respectively, σ_{ion} is the cross-section, N is the neutral gas number density, and ΔV is the cell volume of the computational grid. Ionization cross-sections for different gases versus electron kinetic energy are provided by MAGIC.

In simulations of both configurations, the initial electron density $n_e = 10^4 \text{ cm}^{-3}$ (cosmic background) was set all over the compressor cavity and side arm. For the model configuration, the gas filling the compressor was air, and the coefficients in Eq. (2) as well as mobilities in Eq. (1) were default

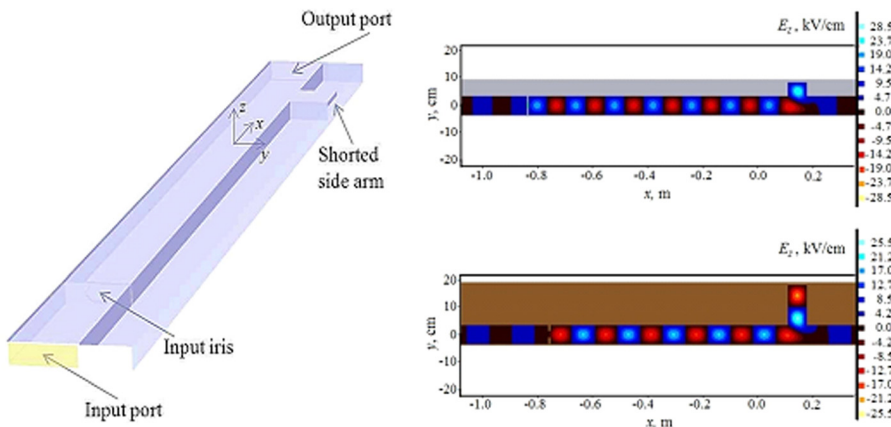


FIG. 1. Schematic view of the simulation region and x - y cross-sections with contour plots of the E_z field component for two different compressor configurations: model (top) and experimental one (bottom).

functions employed for air by MAGIC.¹³ The external ionization rate Q_e in this case was set constant for a fixed time interval within the 8-mm-thick layer crossing the side arm waveguide at the antinode of the RF electric field. For the experimental configuration, to simulate laser triggering of the discharge, as in the experiments,^{14–16} an initial population of particles was set in a small volume around the electric field antinode in the side arm, and Q_e was calculated from Eq. (3). Since in the experiments,^{15,16} the gas filling the system was helium, the attachment rate was set to zero, and the avalanche rate was derived from the empirical formula for the Townsend coefficient for inert gases (see Ref. 2). This derived avalanche rate as a function of the electric field absolute value E is given by

$$\alpha(E) = CE \exp(-DE^{-1/2}), \quad (4)$$

where the pressure-dependent coefficients C and D were calculated using the tabulated data for helium available in Ref. 2, as well as was the electron mobility.

III. SIMULATION RESULTS AND DISCUSSION

A. Model configuration

In studies of the model configuration, we concentrate on the issue of energy balance in the system during the output pulse extraction, particularly on the dynamics of microwave energy absorption in the plasma. In the scope of this model, it was shown in Ref. 11 that for a given input power and external ionization rate, there is an optimal pressure maximizing output power. The efficiency of power extraction, nevertheless, decreases with increasing pressure. It is natural that switching losses increase with increasing pressure as the plasma absorbs more energy due to electron interaction with neutrals. The question, however, remains regarding the dependence of the energy absorption at a fixed high pressure on the rate of external ionization. Is it possible to achieve efficient extraction of the stored microwave energy at high pressure by means of some appropriate discharge triggering technique?

The simulations were performed for air at a pressure of 3×10^5 Pa. The input RF voltage amplitude was set at 15 kV, and the amplitude of the preset RF electric field in its antinode located in the side arm was ≈ 92 kV/cm. Accordingly, the input power was ≈ 225 kW, and the power of the traveling wave component of the preset cavity field (the stored power) was ≈ 14.2 MW. Different constant rates Q_e of external ionization (source term in Eq. (2)) were set for a time interval of 5 ns. After 5 ns and outside the 8-mm-thick layer crossing the waveguide at the field antinode, the source term was set zero. The exact location of the antinode was in the middle of the layer.

The energy balance since the start of external ionization comprises the electromagnetic energy within the system, the energy dissipated in the waveguide walls, the energy absorbed in the plasma, the energy entering the system through the input port (integral of the power flux over time), and the energy leaking through the output port (the energy of the compressor output pulse). In Fig. 2, the energies obtained

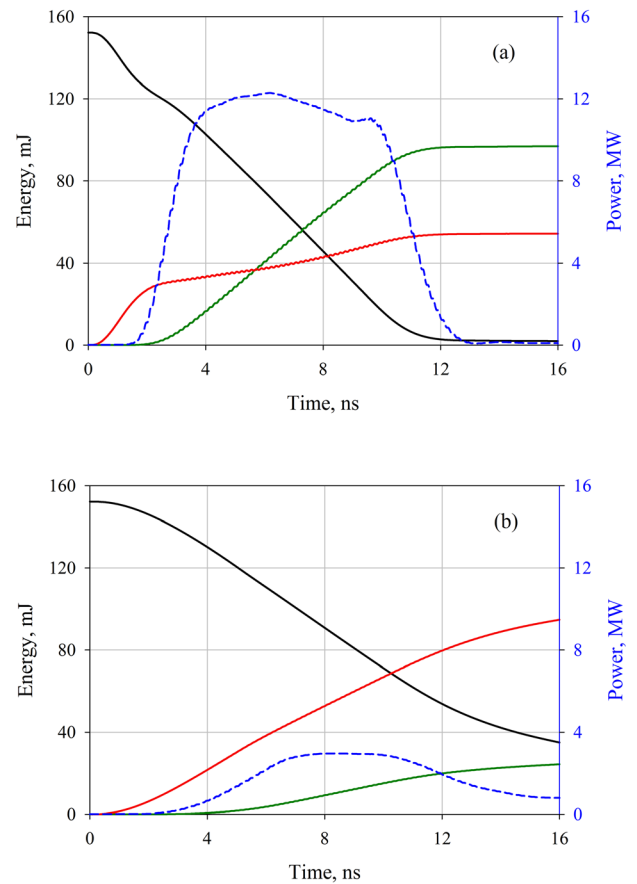


FIG. 2. Dynamics of energy balance. Time dependences of the RF energy within the system (black curves), the energy released from the system (green curves), and the energy absorbed in the plasma (red curves), along with the compressor output power (dashed blue curves) since the start of external ionization. The air pressure is 3×10^5 Pa; the preset stored power in the cavity is ≈ 14.2 MW. The external ionization rate Q_e is set until $t = 5$ ns. (a) $Q_e = 3.16 \times 10^{13} \text{ cm}^{-3}/\text{ns}$; (b) $Q_e = 3.16 \times 10^{12} \text{ cm}^{-3}/\text{ns}$.

in the simulations with two external ionization rates differing by one order of magnitude are presented as a function of time. Also shown in the plots of Fig. 2 is the microwave output power. The energy scattered in the walls and the energy entering the system during the simulation time are not shown, as their contribution to the energy balance is insignificant. It is seen that the higher external ionization rate provides lower switching losses and higher output power of the compressor. The energy absorbed in the plasma for 16 ns is ≈ 54.4 mJ (see Fig. 2(a)), while for the lower ionization rate (Fig. 2(b)) is as high as ≈ 94.7 mJ (the RF energy within the system at $t = 0$ is ≈ 152 mJ, which includes ≈ 139 mJ in the cavity section). Accordingly, the peak output power for the higher Q_e is ≈ 12.3 MW, while for the lower Q_e is only ≈ 3 MW (compare to ≈ 14.2 MW of the stored power). Furthermore, the rise-time of the output pulse is much shorter for the higher Q_e . Let us note here that the dynamics of the energy absorption in the plasma is qualitatively different for these two cases. For the higher external ionization rate, most of the energy is absorbed in the first few nanoseconds, and, after that, the absorption grows rather slowly and finally ends with ending output pulse. For the lower ionization rate, the absorption is first rather low and then grows gradually all over the simulation time. In addition, for the

higher rate of external ionization, the energy of the preset RF field is almost fully spent already by ~ 12 ns, while with the lower rate, a significant part of it remains within the system.

The dynamics of absorption in the plasma is even better illustrated by the time dependences of the absorbed power shown in Fig. 3. It is seen that for the higher external ionization rate (Fig. 3(a)), the absorbed power has a sharp maximum at about 1 ns, which exceeds the power of losses in the plasma at this time in the case of lower ionization rate (Fig. 3(b)) by an order of magnitude. Later in time, however, the absorbed power plotted in Fig. 3(a) is significantly less than that of Fig. 3(b), so that the integral over time is less, as was mentioned above. Also shown in Fig. 3 is the plasma conductivity as the energy absorbed in the plasma is determined by its conductivity and electric field within its volume. One can see that the sharp peak in the absorbed power in Fig. 3(a) corresponds to a conductivity of $\approx 0.14 \Omega^{-1} \text{m}^{-1}$, which is far from being achieved in the case of lower external ionization rate.

It is obvious that at a certain value of the conductivity, the absorbed power is maximized since at zero conductivity, there are no energy losses, while at high conductivity, losses tend to vanish because the electric field is pushed out of the plasma region due to skin effect. This is illustrated by the results of the simulation shown in Fig. 4. One can see how the field decreases with increasing plasma density; the

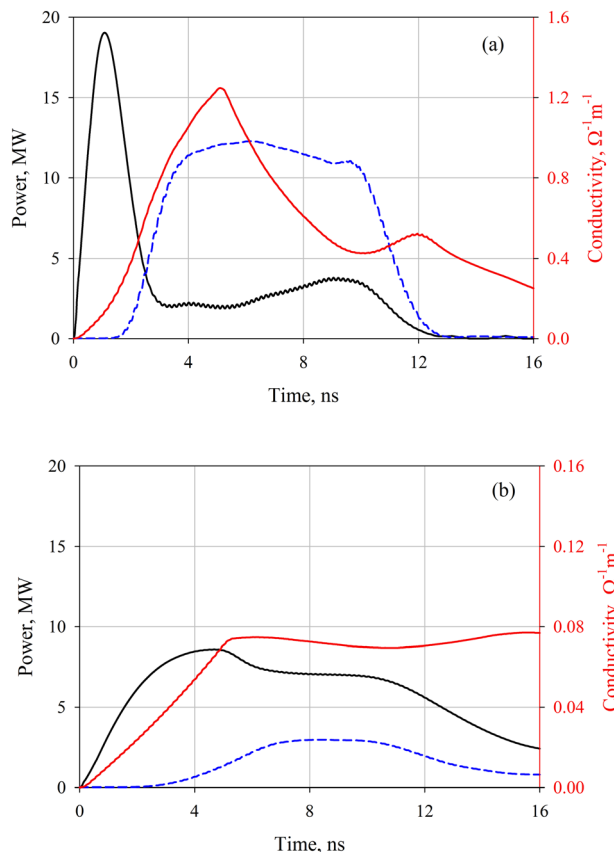


FIG. 3. Time dependences of the power of losses in the plasma (black curves), the compressor output power (dashed blue curves), and the conductivity in the central point of the plasma layer (averaged over the oscillation period, red curves). Plots (a) and (b) correspond to those of Fig. 2 (same simulations).

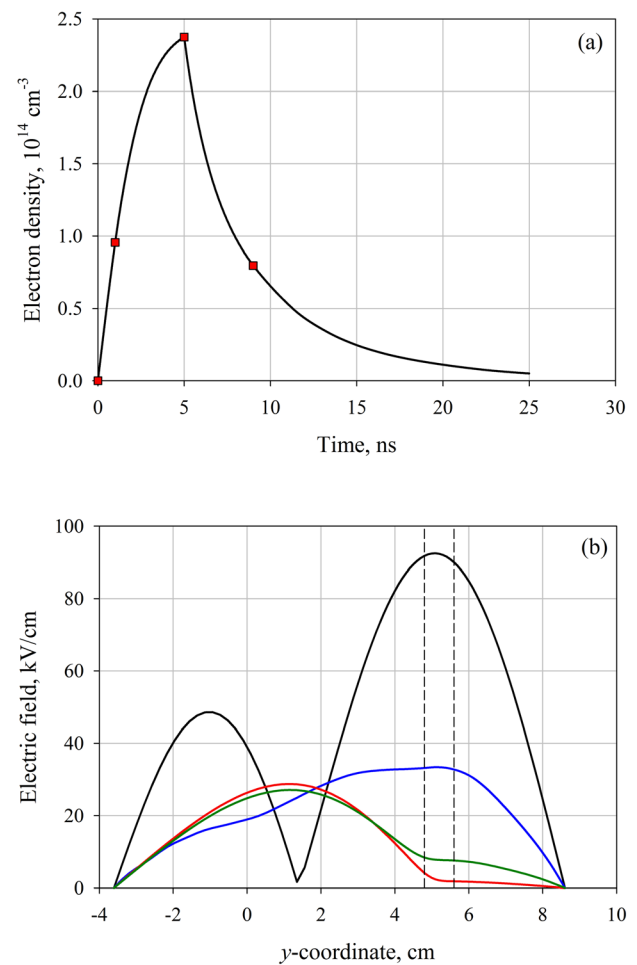


FIG. 4. (a) Temporal evolution of the electron density in the central point of the plasma layer. (b) Profiles of the E_z -field amplitude along the central line of the side arm waveguide before the start of external ionization (black curve), at $t = 1$ ns after the start of ionization (blue curve), at $t = 5$ ns (end of external ionization, red curve), and at $t = 9$ ns (green curve). Simulation with $Q_e = 10^{14} \text{cm}^{-3}/\text{ns}$; all other parameters are the same as in Fig. 2. Dashed lines show the boundaries of the plasma layer. Red squares indicate the time moments, at which the field profiles are presented.

maximal density (and, hence, conductivity) achieved at the end of the external ionization ($t = 5$ ns) corresponds to almost zero electric field within the plasma. Later in time, in the absence of external ionization, the density decreases due to recombination and the electric field once again increases.

As a result, during the external ionization depending on the ionization rate, the plasma conductivity may grow far beyond the value maximizing the power of losses, as in Fig. 3(a), or not reach this value, as in Fig. 3(b). In the former case, the plasma layer can be considered as a good reflector; the rate of energy absorption in it is stabilized at a low level after the initial sharp peak and no longer depends on the conductivity, which continues to change in time. In the latter case, the absorbed power increases with time until the end of external ionization and then remains at the level reached during the energy extraction phase, so that the total energy absorption by the plasma turns out to be very significant.

The portion of stored microwave energy that is absorbed in the plasma is plotted versus the external ionization rate in Fig. 5. It is seen that the maximal absorption shifts towards

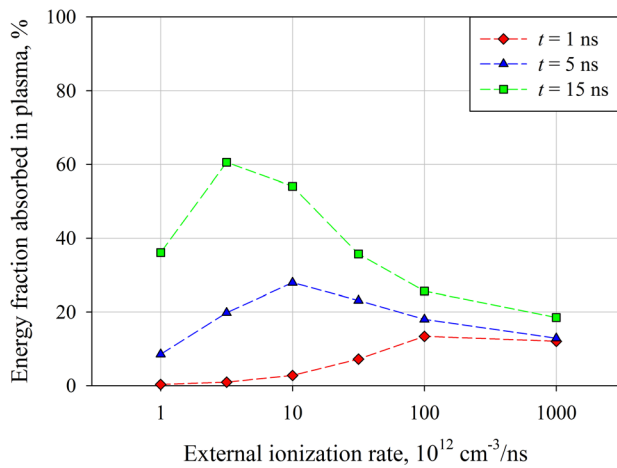


FIG. 5. Dependences of the energy losses in the plasma by different time moments on the external ionization rate Q_e . Simulations with different rates were conducted at the same parameters as those of Fig. 2.

lower rates as time increases. Thus, one can state that increasing ionization rate leads to the increase in the efficiency of the stored energy extraction at gas pressures as high as $3 \times 10^5 \text{ Pa}$. The energy losses, however, do not tend to become negligible. One can see that about 20% of the stored energy is lost at the external ionization rate as high as $10^{15} \text{ cm}^{-3}/\text{ns}$. At such high rate, the plasma conductivity grows very fast. While the value maximizing the absorbed power in Fig. 3(a) (simulation with the rate of $3.16 \times 10^{13} \text{ cm}^{-3}/\text{ns}$) is reached by 1 ns, at the rate of $10^{15} \text{ cm}^{-3}/\text{ns}$, this value is reached at a time much shorter than the period of RF oscillation. Therefore, more time is needed for the RF electric field to be pushed out of the plasma region, and the integral of energy absorption remains rather considerable.

Thus, to reduce the switching losses in a high-power high-gain compressor, one should provide a sufficiently high rate of external ionization. To see if this is achievable, adequate models should be used describing different actual methods for the discharge triggering. Below, we employ one possible approach for producing external ionization—setting an initial population of seed electrons—to model the laser triggering used in our recent experiments.^{14–16}

B. Experimental configuration

In this subsection, we focus on the dynamics of plasma formation in the conditions allowing for the comparison of simulation results with those obtained in the experiments. The objective of the studies was in detailing the mechanism of the influence of self-consistent evolution of the plasma density and RF electric fields in the discharge location on the peak power and waveform of the compressor output pulse. Some simulation results showing good agreement with the experiments on the compressor with laser triggering of the discharge developing in He gas were already reported briefly in Refs. 15 and 16. The results presented below particularly explain the rather low efficiency of the stored power extraction (20–40%) observed in these experiments.

The geometry and preset RF field pattern for the simulations were shown in Fig. 1; the resonant frequency of 2766.8

MHz is in an excellent agreement with the experiment. The RF voltage amplitude at the input port was set lower than for air in Section III A because of the much lower breakdown threshold for helium. In most of the simulations, it was set to be 4.8 kV; the amplitude of the preset RF electric field in the side arm antinodes was $\approx 23 \text{ kV/cm}$, and the stored power in the cavity section was $\approx 860 \text{ kW}$. The fill pressure in these simulations was $2 \times 10^5 \text{ Pa}$, as in the experiments, and the coefficients in the formula (4) for the avalanche rate in He and electron mobility in He were calculated for this pressure giving $C = 3.872 \times 10^6 \text{ cm}/(\text{V s})$, $D = 5.458 \times 10^2 \text{ (V/cm)}^{1/2}$, and $\mu_e = 5.66 \times 10^2 \text{ cm}^2/(\text{V s})$. The electron-ion recombination coefficient in He was set to be $10^{-8} \text{ cm}^3/\text{s}$. The initial population of seed particles (electrons) producing the external ionization was set around the electric field antinode located in the plane distanced at a quarter-guide-wavelength from the side arm shorting plane. It is in this plane that the unfocused laser beam passed in the experiments. The optical imaging of the plasma in the compressor¹⁴ showed that the discharge develops as an expanding filament of $<0.6 \text{ mm}$ transverse dimension, i.e., originates from a single site. Thus, the initial population of particles was set in a small volume of cubic form in the center of the waveguide cross-section. The size of this volume and the uniform charge density in it were variable parameters; the initial velocity of particles was randomly distributed from zero to 10^8 cm/s .

The simulations confirmed that the plasma expands mostly along the RF electric field, forming a filament. The transverse dimension of the filament is determined by the size of the volume initially populated with macro-particles treated by the PIC algorithm. This is illustrated in Fig. 6. It is also seen from Fig. 6 that while the plasma filament extends, the density in its central part becomes lower than that in periphery. It is important to note that the plasma density at $t = 25 \text{ ns}$ is higher for the smaller volume populated with seed particles. The volume size of 1.2 mm was smallest in the simulations as a thinner plasma requires too fine grid for an acceptable runtime. Below (in Figs. 7–9), we present the results of the simulations with the 1.2-mm-volume.

The dynamics of plasma formation is well seen from the density profiles along the z -coordinate across the side arm waveguide in the center of the plasma filament shown in Fig. 7. First, the density increases only within the volume populated with seed particles as the growth due to external ionization is stronger than the growth due to the avalanche rate determined by Eq. (4). Accordingly, at $t = 5 \text{ ns}$ (curve 1), there is a strong gradient of the plasma density at the boundaries of the initial volume. While the density grows further, the region of denser plasma extends and the gradient at its boundaries decreases slightly ($t = 15 \text{ ns}$, curve 2), and at $t = 25 \text{ ns}$, the gradient becomes rather moderate, so that the expressed plasma filament is formed (curve 3).

The mechanism behind the plasma expansion is related to the avalanche process that becomes dominant over the external ionization starting from a certain level of the plasma density, i.e., when the term αn_e in the equation for the density evolution (2) is much greater than the source term Q_e . Thus, the density evolution is determined by the evolution of the avalanche rate (4) depending on the RF electric field,

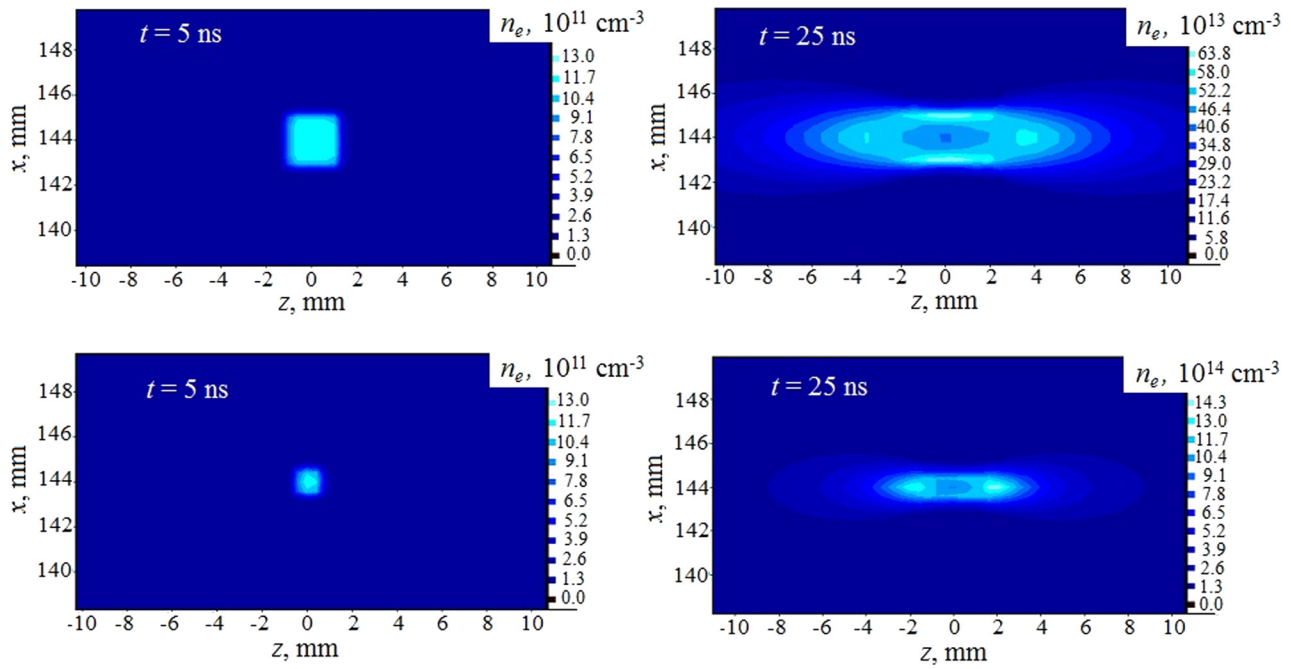


FIG. 6. Contour plots of electron density in z - x plane at y -coordinate of the preset RF electric field antinode at $t = 5$ ns and $t = 25$ ns. The charge density in the cubic volume initially populated with seed particles is 10^{-11} C/cm³. The size of this volume is 2.4 mm (top) and 1.2 mm (bottom).

which, in its turn, depends on the plasma density. In Fig. 8, the non-averaged time dependence of the avalanche rate is presented together with the plasma density evolution at different points along the extending plasma filament. Also shown is the microwave power at the output port that allows one to see the mutual influence of the plasma formation and the output pulse extraction. The avalanche rate in Fig. 8 is at the same point within the initial volume populated with particles as the density plotted by the curve 1. One can see that the density rises very rapidly up to the level $\sim 10^{10}$ cm⁻³, and, after that, the rate of density growth exhibited by the curve 1 becomes the same as that of curves 2–4. As the density reaches the level at which the RF electric field is pushed out of the dense plasma due to the skin effect, the avalanche

rate decreases and the density growth rate in the curve 1 decreases accordingly. At the same time, the field outside the dense plasma region (ahead of the front of the plasma) increases, and, hence, the avalanche rate there increases as well. Accordingly, the density there becomes to grow much faster so that the dense plasma expands along the field, as seen from the behavior of curves 2–4. The extraction of the microwave output pulse begins only when the length of the dense plasma filament becomes sufficiently long, as one can see from the comparison of curves 1–4 and the blue curve for the output power. After the beginning of the energy release, the plasma density is saturated everywhere because the electric field decreases below the level at which it can support the avalanche process.

The evolution of the RF electric field in the center of the plasma volume and its amplitude profile along z -coordinate are shown in Fig. 9. It is seen how the field being first

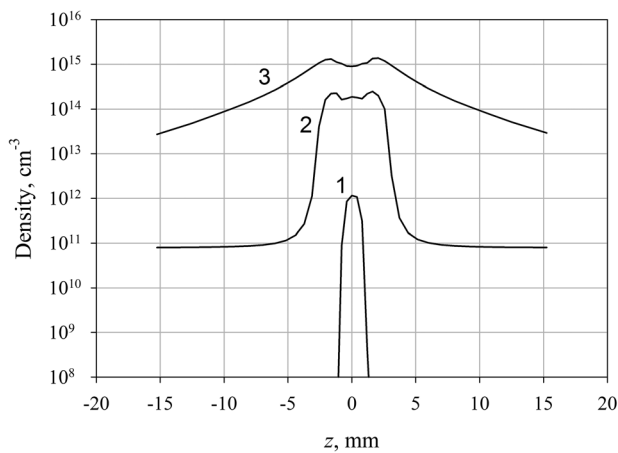


FIG. 7. Plasma density vs. z -coordinate along the centerline of the side arm waveguide cross-section corresponding to the preset RF electric field antinode at different time moments. The initial population of seed particles is set in the 1.2-mm cubic volume with the charge density 10^{-11} C/cm³. $t = 1$ –5 ns; 2–15 ns; 3–25 ns.

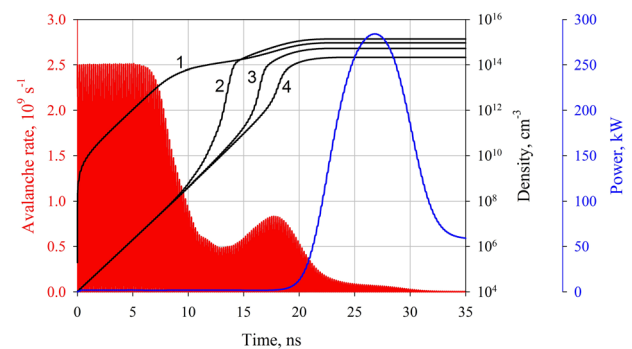


FIG. 8. Temporal evolution of the avalanche rate (red curve) within the volume initially populated with particles and the plasma density (black curves) at different points displaced from the center of the waveguide cross-section in z -coordinate along with the microwave output power (blue curve). Same simulation as of Fig. 7. Observation points for the plasma density are at $z = 1$ –0.4 mm; 2–2 mm; 3–4.4 mm; 4–7 mm.

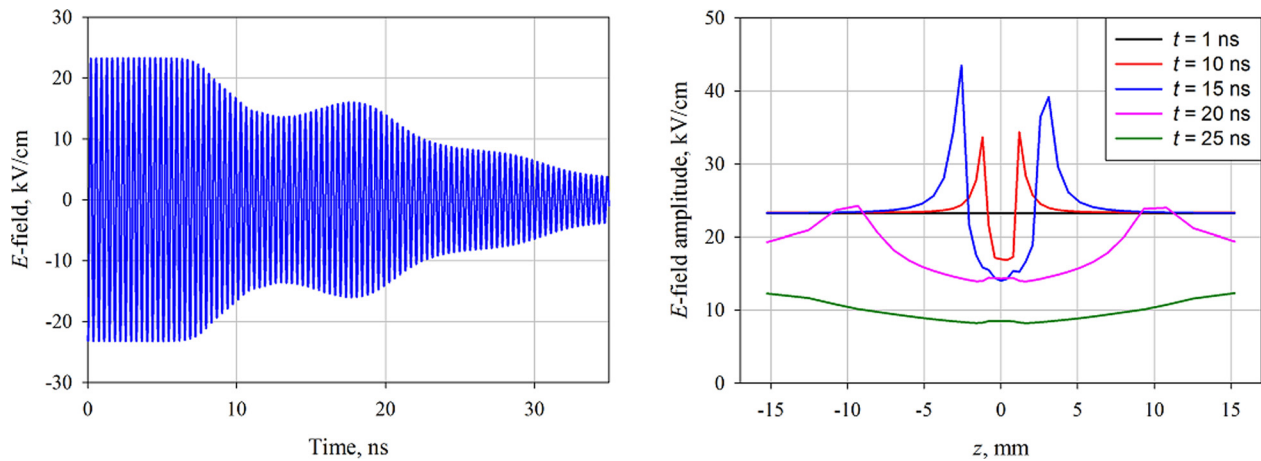


FIG. 9. Left: Time dependence of the electric field within the volume initially populated with particles. Right: Electric field amplitude vs. z -coordinate along the centerline in the plane of the preset electric field antinode at different time moments. Same simulation as of Fig. 7.

uniform (as defined by the TE₁₀-mode structure in a rectangular waveguide) is pushed out of the regions occupied by the dense plasma (right plot) with significant enhancement ahead of the front of the propagating plasma. There is even a time interval in which the field in the center of the plasma volume slightly increases (left plot); the field is pushed out also towards the center when the plasma conductivity there becomes less than in the periphery. After that, however, the compressor cavity goes out of resonance, and the field decreases everywhere as seen in Fig. 9. At $E < 10$ kV/cm, the avalanche is no longer supported—the plasma density no longer rises.

It was shown earlier^{11,14} that the compressor output power increases with increasing plasma density and the volume it occupies. This means that the extraction of the output pulse limits its own power when terminating the rise of the plasma density. The efficiency of power extraction obtained in the simulation for which the compressor output pulse is presented in Fig. 8 is only $\approx 33\%$. Both the peak power and waveform of the output pulse are in excellent agreement with the power and waveform of the pulses registered in the experiments¹⁵ with the close value of the stored power. Moreover, the charge density of seed particles set in this simulation (10^{-11} C/cm³) provides very good agreement with the experiment in the delay time between the moment of the laser beam entering into the system (i.e., creating initial population of seed particles) and the appearance of the output pulse. The good agreement with the experiment in the delay time and satisfactory agreement in the pulse peak power and waveform were also demonstrated in simulations with lower input RF voltages and stored power in preset RF fields (see Ref. 15). It is, therefore, possible to state that setting such a point-like volume of seed particles adequately simulates laser triggering, and the dynamics of plasma formation determines the quality of the output pulses, particularly the low extraction efficiency, obtained in the experiments.

It is obvious that the scenario in which the extraction of the output pulse limits its own power can be avoided if the plasma density and filament length needed for efficient extraction are settled sufficiently fast with respect to the

extraction time, i.e., a round-trip time for a traveling wave along the compressor cavity. As seen in Fig. 8, the time of plasma filament formation is, on the contrary, longer than the output pulse length. Such a situation is inevitable while the external ionization remains negligible in the plasma density evolution, which is determined by the avalanche rate—in our case, by He gas properties. Increasing the external ionization rate Q_e by increasing the charge density in the population of seed particles results in the increase in the plasma density achieved before the ionization rate αn_e begins to dominate over the rate Q_e . This leads to the decrease in the time of plasma formation needed for output pulse extraction. The output power, however, does not increase; it even tends to decrease with increasing charge density of seed particles, as is illustrated in Fig. 10. The peak power of the output pulse for a charge density of 10^{-6} C/cm³ (blue curve 2) is lower than for 10^{-11} C/m³, in spite of the fact that the plasma density within the initial population of seed particles (black curve 2) is significantly higher. This is caused by the fact that the energy release cannot start unless the length of the dense plasma filament is sufficiently long; the plasma

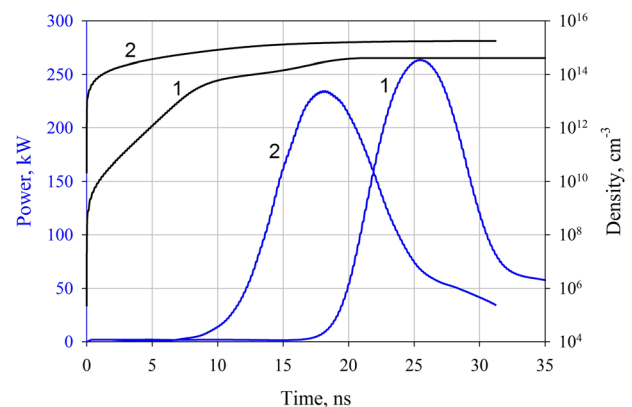


FIG. 10. Microwave output power (blue curves) and plasma density within the volume initially populated with particles (black curves) vs. time. Simulations with the 2.4-mm-size of this volume; the charge density of seed particles is 1 – 10^{-11} C/cm³; 2 – 10^{-6} C/cm³. Other parameters are the same as in Figs. 6–9.

expansion still takes a significant time. Since this time is less than that in the case of the lower charge density, the filament turns out to be shorter and, thus, the output power is lower. One can, therefore, conclude that with the point-like volume of seed particles, it is impossible to achieve a high efficiency of power extraction since it is limited by the finite velocity of plasma expansion.

A different situation takes place if the population of seed particles is set at once as the filament crosses the side arm waveguide over its entire height. Such a configuration models the laser triggering when the unfocused laser beam enters the waveguide along the RF electric field, in contrast to the path across the field. In this case, there is no plasma expansion as the filament is already formed and the plasma density evolution in simulations does not depend on the z -coordinate. A comparison of compressor operation with different laser beam directions was carried out experimentally and in simulations in Ref. 16. It was shown that if the laser beam is directed along the RF electric field, the delay between the plasma discharge initiation and the appearance of the microwave output is shorter, but the compressor output pulse remains practically the same as in the case of laser beam path across the field. This was confirmed in the simulation with the filament-like population of seed particles having a charge density of 10^{-11} C/cm³ and 1.2-mm quadratic cross-section. The energy release for the plasma filament having the maximum possible length starts at the lower density than for the point-like volume of seed particles so that the output power does not considerably change in spite of the larger volume occupied by the plasma. Increasing charge density in the seed particles filament volume, however, leads to the increase in the output pulse power and improves the quality of its waveform, as seen from the results of the simulations presented in Fig. 11. Let us note that the power plotted in curve 2 corresponds to $\approx 75\%$ efficiency of stored power extraction calculated for the “flat-top” of the output pulse. This means that efficient extraction can be achieved in practice by a very significant increase in the laser pulse intensity or by using a powerful laser in the UV spectral range, in contrast with the one employed in Ref. 16.

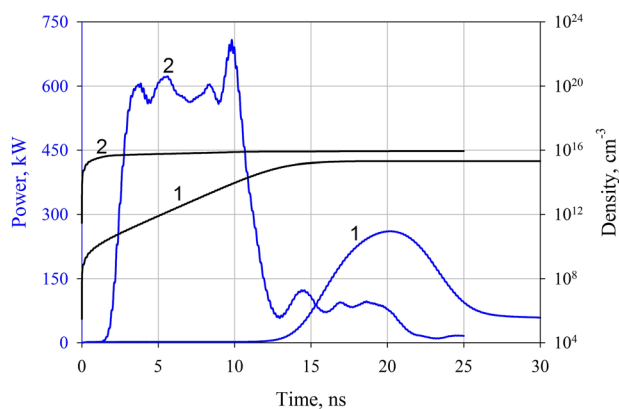


FIG. 11. Same as Fig. 10 for the simulations with seed particles set in the filament of 1.2-mm quadratic cross-section. The charge density of seed particles is $1\text{--}10^{-11}$ C/cm³; $2\text{--}10^{-5}$ C/cm³. Other parameters are the same as in Figs. 6–9.

IV. SUMMARY

The process of RF energy extraction from a microwave pulse compressor with an H-plane waveguide tee-based plasma switch has been studied in numerical simulations accounting for the mutual influence of the plasma density and RF field evolution in time and space. The objective of the studies was to reveal the mechanisms governing the switching losses and waveform of the output pulse in high-gain high-power compressors, in which switching is achieved by a high-pressure gas discharge. We have analyzed the dynamics of both the plasma formation and RF energy absorption in the plasma.

The dynamics of energy absorption in the plasma was investigated by setting the external ionization rate within the layer crossing the side arm waveguide. The external ionization rate determines the plasma density and conductivity, and, thus directly affects the peak power and waveform of the microwave output pulse and energy balance during its extraction. It was found that the higher the ionization rate, the more microwave energy is absorbed by the plasma in the first few nanoseconds, but the absorption for the whole duration of energy release, on the contrary, decreases with increasing external ionization. Nevertheless, switching losses remain significant; particularly, for the external ionization rate as high as 10^{15} cm⁻³/ns set for 5 ns in the 8-mm-thick layer at 3×10^5 Pa gas (air) pressure and 92 kV/cm initial amplitude of the RF electric field, about 20% of the energy stored in the compressor cavity is lost.

The dynamics of plasma formation was investigated using the approach adequately modeling the laser triggering of the discharge—setting the initial population of seed electrons in a small volume around the RF electric field antinode. It was shown that the plasma extends along the field forming a filament whose transverse dimension is set by the dimensions of this volume. The simulations demonstrated good agreement with experimental results obtained for the helium-filled S-band compressor;^{15,16} in particular, the self-consistent evolution of the plasma density and RF electric field explains the rather low efficiency of the stored power extraction observed in these experiments. Three stages of plasma density evolution were found. The first one is an exponential growth up to the level at which the electric field within the plasma region begins to decrease because of the skin effect. Then, the avalanche rate decreases, while the density still rises as the RF energy remains within the cavity. Finally, the stored energy is released, and the electric field becomes insufficient to support the avalanche process. The density no longer rises so that the extraction of the output pulse actually limits its power.

It was shown that such a scenario is inevitable for a point-like volume of the initial population of seed particles. Even if the charge density in this population increases so much that very dense plasma is immediately produced in its volume by the external ionization, the energy release cannot start until the plasma expands up to a certain length. During the time required for this plasma expansion, one obtains RF energy absorption in the plasma, which limits the efficiency of the power extraction. This can be avoided for filament-like seed particle volumes, which model the laser triggering

in the case when the laser beam is directed along the RF electric field. For the filament-like volume, the dense plasma sufficient for the efficient extraction of the stored power can be formed in a time much shorter than the output pulse length. The simulations showed the possibility to obtain $\sim 75\%$ extraction efficiency in the output pulse of much improved waveform quality. The significant increase in the intensity of external ionization produced by the laser beam is necessary for that, and the corresponding measures to be employed for that in practice are being considered now for our future experimental work.

ACKNOWLEDGMENTS

This work was supported in part by the BSF Grant No. 2012038 and under the framework of the KAMEA Program of the Ministry of Immigrant Absorption and the Council for Higher Education, State of Israel.

- ¹A. D. MacDonald, *Microwave Breakdown in Gases* (Wiley, New York, 1966).
- ²Yu. P. Raizer, *Gas Discharge Physics* (Springer-Verlag, Berlin, 1991).
- ³A. L. Vikharev, A. M. Gorbachev, A. V. Kim, and A. L. Kolysko, "Formation of the small-scale structure in a microwave discharge in high-pressure gas," *Sov. J. Plasma Phys.* **18**(8), 554–560 (1992).
- ⁴R. P. Cardoso, T. Belmonte, C. Noel, F. Kosior, and G. Henrion, "Filamentation in argon microwave plasma at atmospheric pressure," *J. Appl. Phys.* **105**, 093306 (2009).
- ⁵Y. Hidaka, E. M. Choi, I. Mastovsky, M. A. Shapiro, J. R. Sirigiri, R. J. Temkin, G. F. Edmiston, A. A. Neuber, and Y. Oda, "Plasma structures observed in gas breakdown using a 1.5 MW, 110 GHz pulsed gyrotron," *Phys. Plasmas* **16**, 055702 (2009).
- ⁶O. I. Voskoboynikova, S. L. Ginzburg, V. F. D'yachenko, and K. V. Khodataev, "Numerical investigation of subcritical microwave discharges in a high-pressure gas," *Tech. Phys.* **47**(8), 955–960 (2002).
- ⁷B. Chaudhuri and J.-P. Boeuf, "Computational studies of filamentary pattern formation in a high power microwave generated air plasma," *IEEE Trans. Plasma Sci.* **38**(9), 2281–2288 (2010).
- ⁸J. Benford, J. A. Swegle, and E. Schamiloglu, *High Power Microwaves*, 2nd Ed. (Taylor & Francis, New York, 2007).
- ⁹A. N. Didenko and Yu. G. Yushkov, *Powerful Microwave Pulses of Nanosecond Duration* (EnergoAtomizdat, Moscow, 1984) (in Russian).
- ¹⁰S. Novikov, Yu. Yushkov, S. Artemenko, P. Chumerin, and R. Shpuntov, "Development of high-power microwave compressors," in *Proceedings of 16th IEEE Pulsed Power Conference (PPPS-2007)*, Albuquerque, NM, 17–22 June 2007 (IEEE, 2007), Vol. 2, pp. 1822–1825.
- ¹¹A. Shlapakovski, L. Beilin, Yu. Bliokh, M. Donskoy, Y. Hadas, E. Schamiloglu, and Ya. E. Krasik, "Numerical simulations of output pulse extraction from a high-power microwave compressor with a plasma switch," *J. Appl. Phys.* **115**, 173302 (2014).
- ¹²B. Goplen, L. Ludeking, D. Smithe, and G. Warren, "User configurable MAGIC code for electromagnetic PIC calculations," *Comput. Phys. Commun.* **87**(1/2), 54–86 (1995).
- ¹³A. J. Woods and L. D. Ludeking, "MAGIC electromagnetic FDTD-PIC code dense plasma model comparison with LSP," *Open Plasma Phys. J.* **3**, 73–77 (2010).
- ¹⁴L. Beilin, A. Shlapakovski, M. Donskoy, Y. Hadas, U. Dai, and Ya. E. Krasik, "Fast-framing optical imaging of plasma formation in resonant microwave pulse compressor," *IEEE Trans. Plasma Sci.* **42**(5), 1346–1352 (2014).
- ¹⁵L. Beilin, A. Shlapakovski, M. Donskoy, T. Queller, and Ya. E. Krasik, "Plasma density temporal evolution in a high-power microwave pulse compressor switch," *Europhys. Lett.* **109**, 25001 (2015).
- ¹⁶A. Shlapakovski, L. Beilin, Y. Hadas, E. Schamiloglu, and Ya. E. Krasik, "Operation of a microwave pulse compressor with a laser-triggered plasma switch at different laser beam directions," *IEEE Trans. Plasma Sci.* **43**(7), 2140–2145 (2015).
- ¹⁷G. D. Stimson, "Practical HPM generation using time domain pulse compression," paper presented at the International Workshop High Power Microwave Generation and Pulse Shortening, Edinburgh, UK, 10–12 June 1997.
- ¹⁸E. G. Farr, L. H. Bowen, W. D. Prather, and C. E. Baum, "Microwave pulse compression experiments at low and high power," *Circuit and Electromagnetic System Design Notes*, Note 63, January 2010.